

Hydrogen Bond Strength Dictates the Rate-Limiting Steps of Diffusion in Proton-Conducting Perovskites: A Critical Length Perspective

Hang Ma,¹ Ying Liang,^{1,2} Tianxing Ma,^{1,2,*} Jiajun Linghu,^{3,†} and Zhi-Peng Li^{4,‡}

¹*School of Physics and Astronomy, Beijing Normal University, Beijing 100875, China*

²*Key Laboratory of Multiscale Spin Physics (Ministry of Education), Beijing Normal University, Beijing 100875, China*

³*Xian 100875, China*

⁴*Frontier Science Center for Flexible Electronics, Xi'an Institute of Flexible Electronics, Northwestern Polytechnical University, 127 Youyi West Road, Xi'an, Shaanxi, 710072, China*

(Dated: Version 16.0 – March 11, 2025)

Proton-conducting solid oxide fuel cells (PC-SOFCs) are pivotal for their high proton conductivity and superior performance. The proton conduction mechanism is commonly described by the Grotthuss mechanism, involving proton rotation and transfer. While proton transfer is often considered the rate-limiting step, the underlying reasons remain unclear. Through density functional theory calculations on undoped, A-site doped, and B-site doped BaHfO₃ systems, we demonstrate that the rate-limiting nature of proton transfer stems from the formation of weaker hydrogen bonds. In systems with strong hydrogen bonds, proton rotation becomes non-negligible. We identify a critical hydrogen bond length that distinguishes strong from weak bonds, with shorter lengths correlating with distorted perovskite structures and configurations deviating from cubic. This insight into the necessity of rotation is crucial for screening and optimizing materials with superior proton conduction properties.

Introduction Decarbonization requires urgent advancements in clean energy, yet fossil fuels still account for 81% of global energy consumption[1]. Proton-conducting solid oxide fuel cells represent a transformative technology, offering high electrical efficiency (50%) and environmentally friendly operation[2, 3]. Conventional oxygen-ion-conducting SOFCs require temperatures above 800°C, accelerating material degradation [4, 5]. In contrast, PC-SOFCs operate at 400–600°C due to lower proton diffusion barriers, enabling superior conductivity and stability [6]. The key factors determining proton conductivity are proton concentration and diffusion rate. Therefore, investigating the diffusion mechanism of protons in solid oxides is of critical importance.

Proton diffusion in oxides follows the Grotthuss mechanism, involving rotation at the same oxygen sites as well as the intraoctahedral transfer and interoctahedral transfer between oxygen ions within the same and adjacent BO₆ octahedra respectively[7–10]. While most studies focus on transfer as the rate-limiting step[11, 12], attributing this to its higher energy barrier compared to rotation[13–17], which result in the residence time constants differing by more than one order of magnitude[16]. However, the physical origin of this hierarchy remains debated. For instance, weaker hydrogen bonds[17] and partial hydrogen bond retention during rotation[15] have been proposed but lack quantitative validation. Especially in some distorted perovskites, the rotation process cannot be ignored(e.g., SrCeO₃[17], BaCe_{1-x}Gd_xO_{3-x/2}[18]). Resolving these ambiguity require a unified framework linking hydrogen bonding, lattice distortion, and energy barriers. Therefore, the mi-

croscopic mechanisms of proton rotation and transfer need to be clarified firstly. For the proton transfer process, molecular dynamics simulations[15, 19] and density functional theory calculations[11, 20] indicate that the thermal vibrations of the two oxygen atoms forming the hydrogen bonds in the BO₆ octahedron facilitate the formation of transient strong hydrogen bonds, followed by proton transfer in the hydrogen-oxygen stretching mode[21, 22]. However, the microscopic process of proton rotation requires further quantitative investigation.

In this study, we decouple the microscopic mechanisms of proton rotation and transfer using density functional theory (DFT) in undoped and doped BaHfO₃ — a corrosion-resistant proton conductor[23, 24], as that detailed in Figs. S1 and S2 of supplemental material(SM). By analyzing the fundamental cause of the energy barrier difference between rotation and transfer as well as its evolution with hydrogen bonds, we demonstrate that the dominance of proton transfer as the rate-limiting step arises from weaker hydrogen bonds. We further identify critical hydrogen bond length that governs whether rotation barriers influence diffusion kinetics. This threshold correlates with structural distortion and deviation from cubic symmetry: systems with these features exhibit shorter hydrogen bonds, necessitating concurrent consideration of rotation. Our findings establish a criterion for evaluating the role of proton rotation in diffusion, aiding in the discovery of high-conductivity electrolytes and the optimization of proton conduction in SOFCs. Furthermore, the analytical approach in this study provides deeper insights into the proton-lattice coupling mecha-

nisms of proton rotation and transfer[21, 25–27].

Method All density functional theory (DFT) calculations were performed using the Vienna Ab Initio Simulation Package (VASP)[28, 29] with the projector augmented wave (PAW) method[30]. The Perdew-Burke-Ernzerhof (PBE) generalized gradient approximation (GGA)[31] exchange-correlation functional was employed. A plane wave basis set with a cutoff energy of 520 eV was used for all calculations. Atomic relaxation was conducted using the conjugate gradient algorithm until the maximum force on any atom fell below 0.01 eV/Å. For k -point sampling, we adopted the Monkhorst-Pack scheme[32] with a grid spacing of 0.028 Å⁻¹. The optimized lattice constants for the BaHfO₃ unit cell were determined to be $a = b = c = 4.20$ Å, showing excellent agreement with both the Materials Project database value ($a = b = c = 4.17$ Å) and previously reported literature values ($a = b = c = 4.209$ Å)[33]. Proton migration barriers were computed in a $2 \times 2 \times 2$ supercell configuration using the climbing image nudged elastic band (CI-NEB) method[34]. During the NEB calculations, structural optimization of each image was restricted to atomic coordinate relaxations while maintaining fixed lattice parameters.

Results and discussions Both the rotation and transfer processes involve the interaction between protons and the crystal lattice[8, 19, 21, 25, 26]. Based on Jing et al.’s research on the origin of proton diffusion energy barriers [20], we calculated the energy barriers for the outward O_i -B- O_f bending motion and the hydroxide ion reorientation that contribute to proton rotation in the ABO₃ structure(Fig. 1a,b). Here, O_i and O_f denote the initial and final oxygen sites of proton transfer, respectively. For proton transfer, as that shown in Figs.1(c,d), we calculated the energy barriers associated with the inward O_i -B- O_f bending motion and the proton jumping (computational details are provided in the Supporting Information). As illustrated in Fig. S2 of SM, for the BaHfO₃ system, the total energy barrier for proton rotation, based on the outward O_i -B- O_f bending motion and the hydroxide ion reorientation, is 0.15 eV, consistent with CI-NEB calculations. Similarly, for proton transfer, the total energy barrier, derived from the inward O_i -B- O_f bending motion and the proton jumping, is 0.28 eV, also aligning with the CI-NEB calculation result of 0.28 eV. In all studied A-site (M_a =Sr²⁺,K⁺,Rb⁺,Cs⁺) and B-site (M_b =Mg³⁺,Ga³⁺,Sc³⁺,In³⁺,Y³⁺) doped systems, the results of the stepwise calculations remain in agreement with CI-NEB calculations (Fig. 2a,b). This consistency confirms the proton-lattice coupling mechanism for both proton rotation and transfer.

As shown in Fig. 3, presenting energy barrier data for the elementary steps of proton rotation and transfer, the energy cost of O_i -B- O_f bending consistently exceeds that of proton reorientation and jumping, highlighting its dominant contribution to the total energy barrier. This

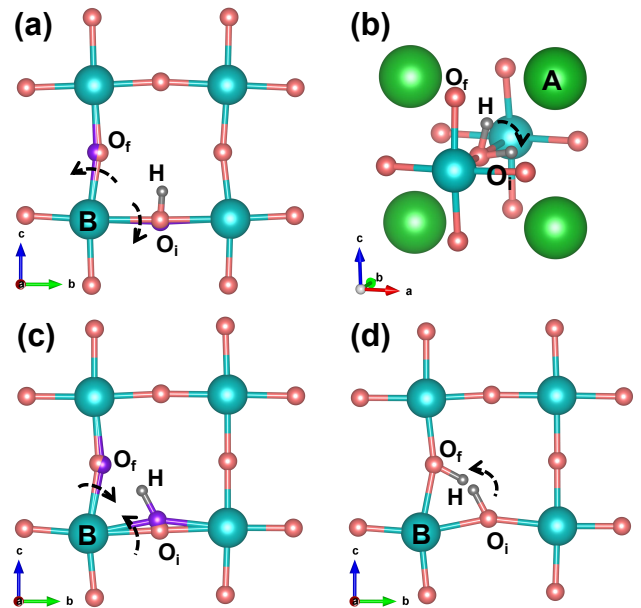


FIG. 1. The first row represents the elementary steps underlying proton rotation and the second row represents the elementary steps underlying proton transfer. (a) Schematic of outward O_i -B- O_f bending during proton rotation. (b) Schematic of hydroxide ion reorientation around A-site ion. (c) Schematic of inward O_i -B- O_f bending during proton transfer. (d) Schematic of proton jumping. The pink balls represent the oxygen atoms before the outward/inward bending, and the purple balls represent the oxygen atoms after the outward/inward bending.

underscores the critical role of lattice bending in both processes. Theoretical work by Kreuer et al.[15] demonstrated that the O_i -B- O_f bending mode reduces the total proton transfer energy barrier. For proton rotation, our CI-NEB calculations confirm that the energy barrier with outward O_i -B- O_f bending is lower than in the absence of this proton-lattice coupling mechanism (Fig.2c). This reduction occurs because the outward O_i -B- O_f bending facilitates the breaking of the hydrogen bond between the proton and the acceptor oxygen O_f , allowing the proton to rotate around the A-site ion with a lower energy barrier, and the barrier for this process arises from the weak Coulomb repulsion with the A-site ion.

The analysis also indicates that the height of bending-mediated energy barriers governing proton rotation and transfer processes is determined by the facility of hydrogen bond rupture and reformation. At finite temperatures, thermal vibrational modes primarily drive lattice distortions associated with bending [27]. When thermal fluctuations shorten the donor-acceptor oxygen distance below a critical threshold, strong hydrogen bonds form, activating proton transfer. Conversely, excessive expansion disrupts hydrogen bonding, facilitating proton reorientation via rotation diffusion. This dynamical interplay reveals the crucial role of lattice compliance in

enabling proton transport through thermally driven hydrogen bond network reorganization[9].

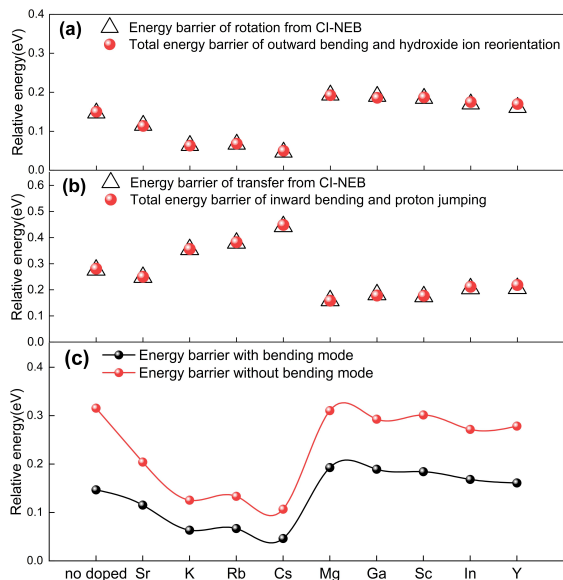


FIG. 2. (a) A comparison of the proton rotation energy barriers by the CI-NEB method and the sum of the energy barriers corresponding to the two steps: outward O_i -B- O_f bending and the hydroxide ion reorientation in pristine and A-site ($M_a = \text{Sr}^{2+}, \text{K}^+, \text{Rb}^+, \text{Cs}^+$), and B-site ($M_b = \text{Mg}^{2+}, \text{Ga}^{3+}, \text{Sc}^{3+}, \text{In}^{3+}, \text{Y}^{3+}$) doped systems. (b) A comparison of the proton transfer energy barriers obtained directly from the CI-NEB calculations with the sum of energy barriers corresponding to the inward O_i -B- O_f bending and the proton jumping. (c) A comparison between the rotation energy barrier with and without the outward O_i -B- O_f bending.

Understanding the microscopic mechanisms of proton rotation and transfer allows for an atomic-level analysis of their kinetic hierarchy. As established in previous studies[13–17], proton transfer typically dominates the rate-limiting step due to its significantly higher energy barriers than that of rotation. Transition state theory[22] defines the residence time for these processes as

$$\tau = \Gamma^{-1} = \nu_0^{-1} e^{\frac{E}{kT}} \quad (1)$$

where Γ is the probability of rotation or transfer, k is the Boltzmann constant, T is the temperature, ν_0 represents the attempt frequency and E is the activation energy. The exponential dependence amplifies even moderate energy differences of 0.13 eV between transfer and rotation suffices to create an order-of-magnitude separation in τ , establishing transfer as the bottleneck in proton diffusion for intermediate-temperature solid oxide fuel cells at $T = 500$ K, attempt frequencies $\nu_0^{rot} = 1500 \text{ cm}^{-1}$ for rotation and $\nu_0^{trans} = 3000 \text{ cm}^{-1}$ for transfer[18]. Notably, the difference between the transfer and rotation energy barriers exceeds this value in most proton-conducting oxides[17, 35], including our first principles calculations

for BaHfO_3 : At 500 K, $\Delta_{\text{energy barriers}} = E_{rot} - E_{trans} = -0.13 \text{ eV}$, resulting in $\tau_{trans}/\tau_{rot} = 10$ and confirming the transfer-dominated kinetics.

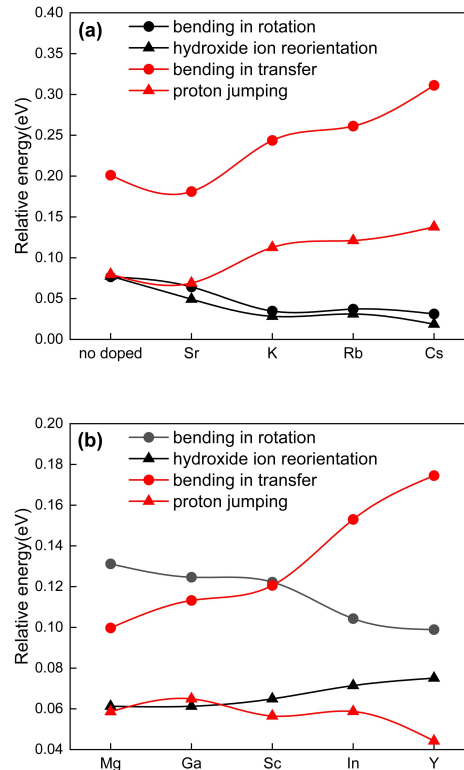


FIG. 3. (a) The energy barrier for the elementary steps underlying proton rotation and transfer in the BaHfO_3 and all A-site ($M_a = \text{Sr}^{2+}, \text{K}^+, \text{Rb}^+, \text{Cs}^+$) doped systems in this study. (b) The energy barrier for the elementary steps underlying proton rotation and transfer in B-site ($M_b = \text{Mg}^{3+}, \text{Ga}^{3+}, \text{Sc}^{3+}, \text{In}^{3+}, \text{Y}^{3+}$) doped systems.

The origin of the higher transfer energy barrier relative to rotation processes can be traced to distinct hydrogen bond dynamics. In BaHfO_3 , analysis of the elementary steps (Fig.3a) reveals that the visible disparity emerges during O_i -B- O_f bending processes for rotation and transfer. As established earlier, these bending-related barriers directly correlate with hydrogen bond reorganization energetics. Therefore, the equilibrium hydrogen bond length of 2.15 Å in BaHfO_3 signifies weak bonding interactions, making the barrier for hydrogen bond rupture during rotation easier compared to the formation of stronger transient hydrogen bonds required for transfer. And this asymmetry in energy barrier yields a factor difference of 10 in residence times (τ_{trans}/τ_{rot}) at 500 K (Table 1), making the dominance of transfer as the rate-limiting step. These results establish hydrogen bond strength as the primary reason for the energy barrier difference in the kinetic hierarchy between rotation and transfer.

To isolate the effects of hydrogen bond, we systematically investigate A-site doped

BaHfO₃(M_a=Sr²⁺,K⁺,Rb⁺,Cs⁺) where dopant-proton interactions influence hydrogen bond strength. Monovalent dopants (e.g.,K⁺,Rb⁺,Cs⁺) exhibit reduced Coulomb repulsion with protons compared to divalent Ba²⁺, creating a net electrostatic attraction that shifts protons toward the dopant (Fig.S3). This configuration weakens hydrogen bonds with acceptor oxygen ions (2.18–2.25 Å vs.2.15 Å in undoped BaHfO₃.) Isovalent Sr²⁺ (ionic radius = 1.44 Å) induces lattice contraction yet retains similarly elongated hydrogen bonds (2.14 Å, Table I). Critically, all doped systems exhibit $\Delta_{energy\ barriers} < -0.13eV$ (Table I), ensuring $\tau_{trans}/\tau_{rot} > 10$ at 500 K. This universal hierarchy further confirms transfer-dominated kinetics across weak hydrogen bond regimes.

Fig. 3(a) reveals a universal phenomenon across A-site doped systems: While distinct energy barriers emerge for hydroxide reorientation (rotation) and proton jumping (transfer), the O_i-B-O_f bending barrier, governed by hydrogen bond strength, remains the dominant factor. The reorientation or interactions and bond-bending processes exhibit cooperative interplay. Table I further demonstrates a systematic correlation: the weaker the formed hydrogen bonds (increasing bond length from 2.14 Å in Sr²⁺ doped to 2.25 Å in Cs⁺ doped systems), the greater the transfer-rotation barrier difference ($|\Delta_{energy\ barriers}|$). Notably, despite lattice contraction, Sr²⁺ doping yields $\Delta_{energy\ barriers} = 0.13eV$, mirroring undoped BaHfO₃ due to comparable hydrogen bond lengths. These results establishes hydrogen bond weakness as the primary driver of large transfer-rotation barrier difference, which universally enforces transfer-dominated kinetics across all A-site doped systems in this study.

TABLE I. The energy barrier differences for rotation and transfer $\Delta_{energy\ barriers}$ ($\Delta_{energy\ barriers} = E_{rot} - E_{trans}$) as well as the hydrogen bond length H...O_f between the proton and the acceptor oxygen ion O_f in the BaHfO₃ system, A-site doped(M_a=Sr²⁺,K⁺,Rb⁺,Cs⁺), and B-site doped(M_b=Mg³⁺,Ga³⁺,Sc³⁺,In³⁺,Y³⁺) systems

Dopant	$\Delta_{energy\ barriers}(eV)$	H...O _f (Å)
no doped	-0.13	2.15
Sr	-0.13	2.11
K	-0.29	2.31
Rb	-0.31	2.32
Cs	-0.40	2.38
Mg	0.03	1.74
Ga	0.01	1.78
Sc	0.01	1.83
In	-0.03	1.95
Y	-0.04	1.97

Our earlier analysis revealed that weak hydrogen bonds in undoped BaHfO₃ result in proton rotation energy barriers significantly lower than transfer barriers. In contrast, systems with strong hydrogen bonds, achieved through B-site doping (M_b=Mg²⁺,Ga³⁺,Sc³⁺,In³⁺,Y³⁺), display significantly different behavior. The reduced Coulomb repulsion between dopants (divalent/trivalent) and protons compared to tetravalent Hf⁴⁺ induces proton tilting toward dopant ions, forming near-linear O_i-HO_f configurations (Fig. S4). This strengthens and shortens the HO_f hydrogen bond (1.83–1.95 Å), as quantified in Table I. Crucially, for Mg²⁺, Ga³⁺, and Sc³⁺ doped systems, rotation barriers now exceed transfer barriers, while In³⁺ and Y³⁺ doping yields $\Delta_{energy\ barriers} > -0.13eV$ at 500 K. This inversion demonstrates that proton transfer no longer universally dictates the rate-limiting step in strongly hydrogen-bonded systems.

Fig. 3(b) highlights the dominant role of O_i-B-O_f bending in determining $\Delta_{energy\ barriers}$ across all B-site dopants. And similar to the trend in the total energy barrier difference, this bending mode energy discrepancy, directly correlating with hydrogen bond strength, reverses sign between Sc³⁺ (H...O_f = 1.83Å) and In³⁺ (H...O_f = 1.95Å) doping. This further confirms that hydrogen bond governs the primary determinant of the kinetic hierarchy in the rotation and transfer energy barriers.

From the previous studies, it can be concluded that at 500K, when weak hydrogen bonds are formed by A-site doping (weaker than in the undoped system), the difference between the rotation and transfer energy barriers is large, making transfer-dominated kinetics. However, when strong hydrogen bonds are formed by B-site doping (stronger than in the undoped system), the rotation and transfer energy barriers become comparable, and thus the transfer cannot be considered as the rate-limiting step. To establish quantitative criteria for this kinetic hierarchy of rotation and transfer, we performed quadratic polynomial fits (Fig. 4) relating H...O_f lengths to $\Delta_{energy\ barriers}$. Defining the critical threshold where rotation becomes non-negligible ($\tau_{trans}/\tau_{rot} = 10$), based on the critical energy barrier difference derived from Equation(1), we find critical H...O_f lengths of 2.08 Å(400 K), 2.13 Å (500 K), and 2.16 Å (600 K). Notably, systems below these thresholds—including B-site doped BaHfO₃ and BaZrO₃ systems, distorted cerates like SrCeO₃, both exhibiting significant octahedral tilting (Fig. S4, Fig. S5), and orthorhombic BaHfO₃(Table S2, obtained by compressing the cubic structure along the *xy* direction). Thus the distorted(octahedral tilting) and non-cubic perovskites, which facilitate strong hydrogen bonds, render rotation and transfer energetically comparable, making the rotation becomes non-negligible.

Summary Our results demonstrate hydrogen bond strength as the decisive factor governing proton diffusion-limiting steps in perovskites. Weak H...O_f bonds (lengths > 2.16 Å) maintain rotation barriers substan-

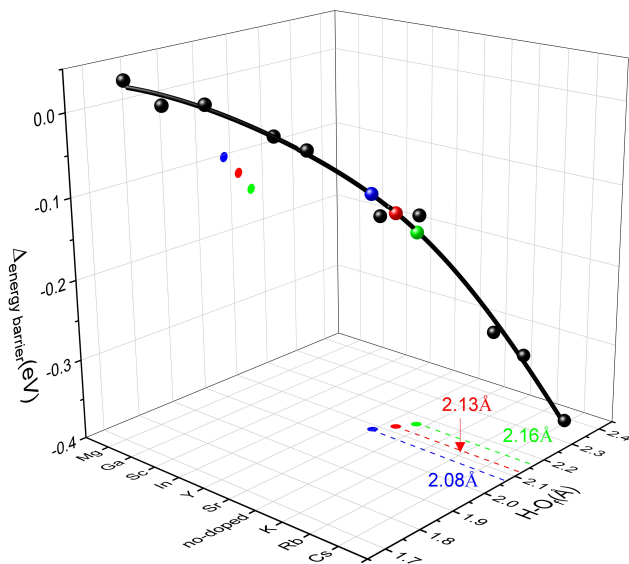


FIG. 4. A quadratic polynomial fitting of the hydrogen bond lengths and the difference barriers between the rotation and transfer energy barriers for undoped, A-site doped ($M_a = \text{Sr}^{2+}, \text{K}^+, \text{Rb}^+, \text{Cs}^+$) and B-site doped ($M_b = \text{Mg}^{3+}, \text{Ga}^{3+}, \text{Sc}^{3+}, \text{In}^{3+}, \text{Y}^{3+}$) BaHfO_3 system. The black dots represent the raw data used for the fitting, while the blue, red, and green dots correspond to the critical points where the transfer can no longer be considered the rate-limiting step at temperatures of 400K, 500K, and 600K, respectively.

tially below transfer barriers, preserving proton transfer as the rate-limiting step. Conversely, strong hydrogen bonds ($< 2.08\text{\AA}$) lower the transfer-rotation energy difference below 0.1 eV , requiring explicit consideration of rotation dynamics. Systems with hydrogen bond lengths smaller than this transition generally exhibit distorted perovskite structures and deviate from the cubic configuration (e.g., B-site doped BaHfO_3 and BaZrO_3 , orthorhombic BaHfO_3 , SrCeO_3). (Fig. S4, Fig. S5)

The identified critical $\text{H}\dots\text{O}_f$ distances ($2.08\text{--}2.16\text{ \AA}$) provide a quantitative structural descriptor for predicting conduction mechanisms. This criterion resolves debates about whether rotation steps need to be considered in proton-conducting oxides, aiding in optimizing the critical steps of proton conduction in SOFCs and screening rational materials experimentally, where the transfer barrier of the material is comparable to the rotation barrier in kinetic hierarchy, allowing protons predominantly to diffuse over long distances through transfer[36].

Acknowledgements: This work was supported by the Double First-Class Construction Fund for Teacher Development Projects (0515024GH0201201 and 0515024SH0201201), Shaanxi Provincial Key Research and Development Plan (2024GX-YBXM-456), National Natural Science Foundation of China (12404463 and 12474218), and Beijing Natural Science Foundation (No.

1242022).

* txma@bnu.edu.cn

† linghujiajun@chd.edu.cn

‡ iamzpli@nwpu.edu.cn

- [1] J. Abe, A. Popoola, E. Ajenifuja, and O. Popoola, Hydrogen energy, economy and storage: Review and recommendation, *International Journal of Hydrogen Energy* **44**, 15072 (2019).
- [2] Q. Xu, Z. Guo, L. Xia, Q. He, Z. Li, I. Temitope Bello, K. Zheng, and M. Ni, A comprehensive review of solid oxide fuel cells operating on various promising alternative fuels, *Energy Conversion and Management* **253**, 115175 (2022).
- [3] Y. Bicer and F. Khalid, Life cycle environmental impact comparison of solid oxide fuel cells fueled by natural gas, hydrogen, ammonia and methanol for combined heat and power generation, *International Journal of Hydrogen Energy* **45**, 3670 (2020).
- [4] B. Timurkutluk, C. Timurkutluk, M. D. Mat, and Y. Kaplan, A review on cell/stack designs for high performance solid oxide fuel cells, *Renewable and Sustainable Energy Reviews* **56**, 1101 (2016).
- [5] S. Ryu, I. W. Choi, Y. J. Kim, S. Lee, W. Jeong, W. Yu, G. Y. Cho, and S. W. Cha, Nanocrystal engineering of thin-film yttria-stabilized zirconia electrolytes for low-temperature solid-oxide fuel cells, *ACS Applied Materials & Interfaces* **15**, 42659 (2023).
- [6] H. Ding, W. Wu, C. Jiang, Y. Ding, W. Bian, B. Hu, P. Singh, C. J. Orme, L. Wang, Y. Zhang, *et al.*, Self-sustainable protonic ceramic electrochemical cells using a triple conducting electrode for hydrogen and power production, *Nature communications* **11**, 1907 (2020).
- [7] N. Agmon, The grotthuss mechanism, *Chemical Physics Letters* **244**, 456 (1995).
- [8] K. Kreuer, On the complexity of proton conduction phenomena, *Solid State Ionics* **136-137**, 149 (2000).
- [9] T. C. Berkelbach, H.-S. Lee, and M. E. Tuckerman, Concerted hydrogen-bond dynamics in the transport mechanism of the hydrated proton: A first-principles molecular dynamics study, *Phys. Rev. Lett.* **103**, 238302 (2009).
- [10] I. Popov, Z. Zhu, A. R. Young-Gonzales, R. L. Sacci, E. Mamontov, C. Gainaru, S. J. Paddison, and A. P. Sokolov, Search for a grotthuss mechanism through the observation of proton transfer, *Communications Chemistry* **6**, 77 (2023).
- [11] B. Merinov and I. Goddard, William, Proton diffusion pathways and rates in y-doped bazro_3 solid oxide electrolyte from quantum mechanics, *The Journal of Chemical Physics* **130**, 194707 (2009).
- [12] J. Linghu, M. K. Butt, P. Feng, K. Yang, F. Ye, T. Yang, J. Che, M. Yang, and Z. Li, Multivalent metal perovskite ybcoo_3 as a novel proton-conducting electrolyte for solid oxide fuel cells, *Ceramics International* **51**, 2922 (2025).
- [13] M. Pionke, T. Mono, W. Schweika, T. Springer, and H. Schober, Investigation of the hydrogen mobility in a mixed perovskite: $\text{Ba}[\text{ca}(1+x)/3\text{nb}(2-x)/3]\text{o}_{3-x/2}$ by quasielastic neutron scattering, *Solid State Ionics* **97**, 497 (1997).
- [14] T. Matzke, U. Stimming, C. Karmonik, M. Soetratmo,

- R. Hempelmann, and F. Güthoff, Quasielastic thermal neutron scattering experiment on the proton conductor $\text{SrCe}_{0.95}\text{Yb}_{0.05}\text{Hf}_{0.02}\text{O}_{2.985}$, *Solid State Ionics* **86-88**, 621 (1996).
- [15] K.-D. Kreuer, A. Fuchs, and J. Maier, Hf isotope effect of proton conductivity and proton conduction mechanism in oxides, *Solid State Ionics* **77**, 157 (1995).
- [16] W. Münch, G. Seifert, K. Kreuer, and J. Maier, A quantum molecular dynamics study of proton conduction phenomena in BaCeO_3 , *Solid State Ionics* **86-88**, 647 (1996).
- [17] W. Münch, K. D. Kreuer, Adams, G. Seifert, and J. Maier, The relation between crystal structure and the formation and mobility of protonic charge carriers in perovskite-type oxides: A case study of γ -doped BaCeO_3 and SrCeO_3 , *Phase Transitions* **68**, 567 (1999).
- [18] J. Hermet, M. Torrent, F. m. c. Bottin, G. Dezanneau, and G. Geneste, Hydrogen diffusion in the protonic conductor $\text{BaCe}_{1-x}\text{Gd}_x\text{O}_{3-\frac{x}{2}}$ from density functional theory, *Phys. Rev. B* **87**, 104303 (2013).
- [19] W. Münch, K.-D. Kreuer, G. Seifert, and J. Maier, Proton diffusion in perovskites: comparison between BaCeO_3 , BaZrO_3 , SrTiO_3 , and CaTiO_3 using quantum molecular dynamics, *Solid State Ionics* **136-137**, 183 (2000).
- [20] Y. Jing and N. Aluru, The role of a-site ion on proton diffusion in perovskite oxides (ABO_3), *Journal of Power Sources* **445**, 227327 (2020).
- [21] E. J. Spahr, L. Wen, M. Stavola, L. A. Boatner, L. C. Feldman, N. H. Tolks, and G. Lüpke, Proton tunneling: A decay channel of the o-h stretch mode in KTAO_3 , *Phys. Rev. Lett.* **102**, 075506 (2009).
- [22] P. Hänggi, P. Talkner, and M. Borkovec, Reaction-rate theory: fifty years after kramers, *Rev. Mod. Phys.* **62**, 251 (1990).
- [23] K. Kato, D. Han, and T. Uda, Transport properties of proton conductive γ -doped BaHfO_3 and Ca or Sr-substituted γ -doped BaZrO_3 , *Journal of the American Ceramic Society* **102**, 1201 (2019).
- [24] S. G. Kang and D. S. Sholl, Characterizing chemical stability and proton conductivity of b-site doped barium hafnate (BaHfO_3) and barium stannate (BaSnO_3) with first principles modeling, *Journal of Alloys and Compounds* **693**, 738 (2017).
- [25] A. Samgin, Lattice-assisted proton motion in perovskite oxides, *Solid State Ionics* **136-137**, 291 (2000).
- [26] P. Du, Q. Chen, Z. Fan, H. Pan, F. G. Haibach, M. A. Gomez, and A. Braun, Cooperative origin of proton pair diffusivity in yttrium substituted barium zirconate, *Communications Physics* **3**, 200 (2020).
- [27] A. Braun and Q. Chen, Experimental neutron scattering evidence for proton polaron in hydrated metal oxide proton conductors, *Nature Communications* **8**, 15830 (2017).
- [28] G. Kresse and J. Furthmüller, Efficiency of ab-initio total energy calculations for metals and semiconductors using a plane-wave basis set, *Computational Materials Science* **6**, 15 (1996).
- [29] G. Kresse and D. Joubert, From ultrasoft pseudopotentials to the projector augmented-wave method, *Phys. Rev. B* **59**, 1758 (1999).
- [30] G. Kresse and J. Furthmüller, Efficient iterative schemes for ab initio total-energy calculations using a plane-wave basis set, *Phys. Rev. B* **54**, 11169 (1996).
- [31] J. P. Perdew, K. Burke, and M. Ernzerhof, Generalized gradient approximation made simple, *Phys. Rev. Lett.* **77**, 3865 (1996).
- [32] H. J. Monkhorst and J. D. Pack, Special points for brillouin-zone integrations, *Phys. Rev. B* **13**, 5188 (1976).
- [33] S. Akhtar, S. M. Alay-e Abbas, S. M. G. Abbas, M. I. Arshad, J. Batool, and N. Amin, First-principles evaluation of electronic and optical properties of (mo, c) codoped BaHfO_3 for applications in photocatalysis, *Journal of Applied Physics* **123**, 161569 (2018).
- [34] G. Henkelman, B. P. Uberuaga, and H. Jónsson, A climbing image nudged elastic band method for finding saddle points and minimum energy paths, *The Journal of Chemical Physics* **113**, 9901 (2000).
- [35] N. Bork, N. Bonanos, J. Rossmeis, and T. Vegge, Simple descriptors for proton-conducting perovskites from density functional theory, *Phys. Rev. B* **82**, 014103 (2010).
- [36] A. Torayev, L. Sperrin, M. A. Gomez, J. A. Kattirtzi, C. Merlet, and C. P. Grey, Local distortions and dynamics in hydrated γ -doped BaZrO_3 , *The Journal of Physical Chemistry C* **124**, 16689 (2020).